

# Orbiting a binary: SPHERE characterisation of the HD 284149 system

M. Bonavita<sup>1,2</sup>, V. D’Orazi<sup>1</sup>, D. Mesa<sup>1</sup>, C. Fontanive<sup>2</sup>, S. Desidera<sup>1</sup>, S. Messina<sup>4</sup>, S. Daemgen<sup>3</sup>, R. Gratton<sup>1</sup>, A. Vigan<sup>5</sup>, M. Bonnefoy<sup>7</sup>, A. Zurlo<sup>5,19</sup>, J. Antichi<sup>13,1</sup>, H. Avenhaus<sup>3,6,16</sup>, A. Baruffolo<sup>1</sup>, J. L. Baudino<sup>18</sup>, J. L. Beuzit<sup>7</sup>, A. Boccaletti<sup>10</sup>, P. Bruno<sup>4</sup>, T. Buey<sup>10</sup>, M. Carillet<sup>19</sup>, E. Cascone<sup>14</sup>, G. Chauvin<sup>7</sup>, R. U. Claudi<sup>1</sup>, V. De Caprio<sup>14</sup>, D. Fantinel<sup>1</sup>, G. Farisato<sup>1</sup>, M. Feldt<sup>6</sup>, R. Galicher<sup>10</sup>, E. Giro<sup>1</sup>, C. Gry<sup>5</sup>, J. Hagelberg<sup>7</sup>, S. Incorvaia<sup>15</sup>, M. Janson<sup>6,9</sup>, M. Jaquet<sup>5</sup>, A. M. Lagrange<sup>7</sup>, M. Langlois<sup>5</sup>, J. Lannier<sup>7</sup>, H. Le Coroller<sup>5</sup>, L. Lessio<sup>1</sup>, R. Ligi<sup>5</sup>, A. L. Maire<sup>6</sup>, F. Menard<sup>7,8</sup>, C. Perrot<sup>10</sup>, S. Peretti<sup>12</sup>, C. Petit<sup>21</sup>, J. Ramos<sup>6</sup>, A. Roux<sup>7</sup>, B. Salasnich<sup>1</sup>, G. Salter<sup>5</sup>, M. Samland<sup>6</sup>, S. Scuderi<sup>4</sup>, J. Schlieder<sup>6,17</sup>, M. Surez<sup>21</sup>, M. Turatto<sup>1</sup>, and L. Weber<sup>12</sup>

<sup>1</sup> INAF – Osservatorio Astronomico di Padova, Vicolo dell’Osservatorio 5, I-35122, Padova, Italy

<sup>2</sup> Institute for Astronomy, The University of Edinburgh, Royal Observatory, Blackford Hill, Edinburgh, EH9 3HJ, U.K.

<sup>3</sup> Institute for Astronomy, ETH Zurich, Wolfgang-Pauli Strasse 27, 8093 Zurich, Switzerland

<sup>4</sup> INAF – Osservatorio Astronomico di Catania, Via Santa Sofia, 78, Catania, Italy

<sup>5</sup> Aix Marseille Univ, CNRS, LAM, Laboratoire d’Astrophysique de Marseille, Marseille, France

<sup>6</sup> Max-Planck Institute for Astronomy, Königstuhl 17, 69117 Heidelberg, Germany

<sup>7</sup> Univ. Grenoble Alpes, CNRS, IPAG, F-38000 Grenoble, France

<sup>8</sup> European Southern Observatory (ESO), Karl-Schwarzschild-Str. 2,85748 Garching, Germany

<sup>9</sup> Department of Astronomy, Stockholm University, AlbaNova University Center, 106 91 Stockholm, Sweden

<sup>10</sup> LESIA, Observatoire de Paris, PSL Research University, CNRS, Sorbonne Universités, UPMC Univ. Paris 06, Univ. Paris Diderot, Sorbonne Paris Cité

<sup>11</sup> Observatoire de Haute-Provence, CNRS, Université d’Aix-Marseille, 04870 Saint-Michel-l’Observatoire, France

<sup>12</sup> Observatoire Astronomique de l’Université de Genève, Chemin des Maillettes 51, 1290 Sauverny, Switzerland

<sup>13</sup> INAF - Osservatorio Astrofisico di Arcetri, L.go E. Fermi 5, 50125 Firenze, Italy

<sup>14</sup> INAF - Osservatorio Astronomico di Capodimonte, Salita Moiariello 16, 80131 Napoli, Italy

<sup>15</sup> INAF-Istituto di Astrofisica Spaziale e Fisica Cosmica di Milano, via E. Bassini 15, 20133 Milano, Italy

<sup>16</sup> Universidad de Chile, Camino el Observatorio, 1515 Santiago, Chile

<sup>17</sup> NASA Goddard Space Flight Center, Greenbelt, MD 20771, USA

<sup>18</sup> Department of Physics, University of Oxford, Parks Rd, Oxford OX1 3PU, UK

<sup>19</sup> Núcleo de Astronomía, Facultad de Ingeniería, Universidad Diego Portales, Av. Ejercito 441, Santiago, Chile

<sup>20</sup> Université Côte d’Azur, OCA, CNRS, Lagrange, France

<sup>21</sup> ONERA (Office National d’Etudes et de Recherches Aéronautiques), B.P.72, F-92322 Chatillon, France

Received / Accepted

## ABSTRACT

**Aims.** In this paper we present the results of the SPHERE observation of the HD 284149 system, aimed at a more detailed characterisation of both the primary and its brown dwarf companion.

**Methods.** We observed HD 284149 in the near-infrared with SPHERE, using the imaging mode (IRDIS+IFS) and the long-slit spectroscopy mode (IRDIS-LSS). The data were reduced using the dedicated SPHERE pipeline, and algorithms such as PCA and TLOCI were applied to reduce the speckle pattern.

**Results.** The IFS images revealed a previously unknown low-mass ( $\sim 0.16 M_{\odot}$ ) stellar companion (HD 284149 B) at  $\sim 0.1''$ , compatible with previously observed radial velocity differences, as well as proper motion differences between Gaia and Tycho-2 measurements. The known brown dwarf companion (HD 284149 b) is clearly visible in the IRDIS images. This allowed us to refine both its photometry and astrometry. The analysis of the medium resolution IRDIS long slit spectra also allowed a refinement of temperature and spectral type estimates. A full reassessment of the age and distance of the system was also performed, leading to more precise values of both mass and semi-major axis.

**Conclusions.** As a result of this study, HD 284149 ABb therefore becomes the latest addition to the (short) list of brown dwarfs on wide circumbinary orbits, providing new evidence to support recent claims that object in such configuration occur with a similar frequency to wide companions to single stars.

**Key words.** Stars: individual: HD 284149, HD 284149 b, HD 284149 B, Stars: brown dwarfs, Stars: binaries: visual, Stars: rotation, Techniques: high angular resolution

## 1. Introduction

Several new sub-stellar companions to nearby young stars have been directly imaged in the last decade, spanning a wide range of masses and separations (see e.g. Chauvin et al. 2005a,b; Marois et al. 2008, 2010; Lagrange et al. 2010; Biller et al. 2010; Carson et al. 2013; Delorme et al. 2013; Rameau et al. 2013; Bailey et al. 2014a; Bonavita et al. 2014; Gauza et al. 2015a; Stone et al. 2016a; Wagner et al. 2016). These objects, some of which have masses near and below  $15M_{Jup}$  (see e.g. Marois et al. 2008, 2010; Lagrange et al. 2010; Rameau et al. 2013; Bailey et al. 2014a; Kraus et al. 2014; Macintosh et al. 2015; Naud et al. 2014; Artigau et al. 2015; Bowler et al. 2017), may represent the bottom end of the stellar companion mass function as well as the top end of the planet population, though both scenarios pose challenges to conventional formation models.

On one hand, the binary star formation process (e.g. Bate et al. 2003) rarely predicts such low mass ratios. On the other hand, the standard core accretion model would struggle to form super-Jupiter planets at  $> 50$  AU. Even though the alternative gravitational instability (GI) model might become more plausible at large separations (see Meru & Bate 2010), especially around more massive stars with larger disks, it is still unclear whether or not such hypothesis is correct (see e.g. Janson et al. 2012).

Some of the most recent GI models (see e.g. Forgan & Rice 2013; Forgan et al. 2015) seem to suggest that the most likely outcome of such formation process is a large fraction of relatively massive objects at large semi-major axis. Such a population would be easily detectable with direct imaging, and the lack of detections can be used to place strong constraints on how frequently disk fragmentation occurs (see e.g. Vigan et al. 2017).

An in depth characterisation of the few known members of this population is therefore highly desirable, but the lack of multi-wavelength spectroscopy and photometry make precise characterisation of these systems quite challenging, leading to poorly constrained values of some fundamental properties such as mass, radius, effective temperature etc.

New dedicated instruments, which allow both precise multi band photometry and low and medium resolution spectroscopy, are now becoming available and allow a better characterisation of low mass companions. SPHERE (Beuzit et al. 2008), the new planet finder mounted at the VLT, is one of those.

SPHERE includes three scientific modules: IFS (Claudi et al. 2008) and IRDIS (Dohlen et al. 2008), both operating in the NIR, and ZIMPOL (Thalmann et al. 2008) which uses visible light instead. The main IRDIFS imaging mode uses the IFS and IRDIS channels simultaneously: low resolution ( $R=50$ ) spectra are obtained with IFS while dual band images (DBI, see Vigan et al. 2010) are taken using the IRDIS H2-H3 filter pair at  $1.593 \mu\text{m}$  and  $1.667 \mu\text{m}$ . Lower resolution but wider spectra can be obtained using the IRDIFS\_EXT mode. In this case the IFS spectra have  $R=30$  and the K1-K2 filter pair is used for IRDIS, taking images at  $2.110 \mu\text{m}$  and  $2.251 \mu\text{m}$ . Finally, IRDIS can be used in long slit spectroscopy (LSS Vigan et al. 2008) mode, supplying medium resolution ( $R=350$ ) and low resolution ( $R=50$ ) spectra. Since the start of operation in December 2014, SPHERE has been used to characterise several directly imaged companions (see e.g. Vigan et al. 2016; Maire et al. 2016a; Bonnefoy et al. 2016; Zurlo et al. 2016; Mesa et al. 2016a).

The brown dwarf companion at  $\sim 3.6''$  from the F8 star HD 284149 was discovered by Bonavita et al. (2014) as part of a direct imaging survey of 74 members the Taurus star forming re-

gion (Daemgen et al. 2015). Together with several other targets of the same survey, HD 284149 has been proposed to be part of the so-called Taurus-Ext association (Luhman et al. 2017; Kraus et al. 2017; Daemgen et al. 2015), a group of stars with similar space position and kinematics of the Taurus star forming region but distinctly older ages. A dedicated age estimate was then performed for HD 284149 by Bonavita et al. (2014), using several youth indicators, leading to an adopted age of  $25^{+25}_{-10}$  Myrs. They therefore finally estimated the mass of HD 284149 b to be  $32^{+18}_{-14} M_{Jup}$ . From the available photometry they were able to infer a spectral type between M8 and L1 and an effective temperature of  $2537^{+95}_{-182}$  K, but no spectroscopic characterisation has been performed up to now, leaving these estimates highly uncertain.

Here we present the result of the observations of HD 284149 performed with SPHERE, aimed at a precise characterisation of the whole system.

Section 2 contains a detailed description of the observations and data reduction while an update to the stellar characteristics given the new information available, including those coming from the Gaia mission, is given in Section 3. The results are described and discussed in Section 4 and include the description of a newly discovered close stellar companion, an update of the astrometry of the known wide brown dwarf companion and the comparison with the models of the medium resolution spectra obtained with the IRDIS LSS mode.

## 2. Observations and data reduction

HD 284149 was observed with SPHERE in IRDIFS mode on 2015-10-25 and with IRDIFS\_EXT mode on 2015-11-27 as part of the SHINE (SpHere INfrared survey for Exoplanet) GTO campaign. The second epoch observations were taken without coronagraph to confirm a faint candidate that was imaged for the first time very close to the edge of the coronagraphic mask in the first observation. In order to take full advantage of the angular differential imaging technique (ADI, see Marois et al. 2006a), for both epochs the target was observed in pupil-stabilised mode to allow the rotation of the field of view. The reduction of all the IRDIS and IFS data sets was performed through the SPHERE Data Center (DC) using the SPHERE Data Reduction and Handling (DRH) automated pipeline (Pavlov et al. 2008). In the case of the IFS data, the DRH pipeline is complemented with additional routines that allow for an improved wavelength calibration as well as for a correction of both coherent and incoherent cross-talk effects (see Mesa et al. 2015; Antichi et al. 2009, for a detailed description on method and theory, respectively). The reduced images are then finally processed using the SHINE Specal pipeline (R. Galicher, private comm.), that provides anamorphism and flux normalisation, as well as speckle correction, using various flavors of angular and spectral differential imaging algorithms. A detailed description of the various tools is given in the following sections in case dedicated routines are applied for the reduction.

Observations of HD 284149 and its brown dwarf companion were also acquired on 2015-02-03 employing the long slit spectroscopic (LSS) mode of the IRDIS instrument. Contrary to the imaging ones, the LSS observations are always performed in field-stabilised mode. This ensures that the object is kept within the slit during the complete integration. Each LSS observing sequence included images taken with the coronagraph, an off-axis reference PSF (that is an image of the target star offset from the coronagraph), and the spectrum of an early-type star used for

telluric calibration. Finally, a series of sky backgrounds was acquired.

Table 1 summarises the main observational setup for all the epochs. The reduced non-coronagraphic images for both IRDIS and IFS are shown in Figure 1.

### 2.1. IFS data

The IFS calibration data (dark, detector flat, spectral position frames, wavelength calibration and instrument flat) were treated using the data reduction and handling (DRH) software (Pavlov et al. 2008).

For the coronagraphic data of 2015-10-25 we obtained a calibrated data cube for each of the 64 frames which were then used to apply the principal component analysis procedure (PCA, see Soummer et al. 2012; Amara & Quanz 2012, for details). They were registered using images with satellite spots symmetrical with respect to the central star (waffles, see e. g. Sivaramakrishnan & Oppenheimer 2006; Marois et al. 2006b; Langlois et al. 2013) and flux calibrated exploiting images taken with the star outside the coronagraph. The PCA routine that was used applies both the Angular Differential Imaging and the Spectral Differential Imaging techniques (ADI and SDI, respectively. See e.g. Marois et al. 2006a). A more detailed description of the reduction procedures can be found in Mesa et al. (2015) and Mesa et al. (2016a).

The non-coronagraphic data of 2015-11-27 were instead binned and stacked in sets of 10, to obtain 160 frames rotated of  $\sim 0.2^\circ$  from each other. This final data cube was reduced in a similar way as the coronagraphic data described above, with the exception of the flux calibration which was not needed, and the centering which was performed using the CNTRD IDL procedure.

Figure 2 shows the limits achieved with the non-coronagraphic observations, both in terms of magnitude and minimum mass of detectable companions.

### 2.2. IRDIS imaging data

Data reduction for the IRDIS data was performed following the procedures described in Zurlo et al. (2014). The IRDIS raw images were pre-reduced performing background subtraction, bad-pixels correction, and flat fielding. In a similar way to what done for the IFS coronagraphic images (see Section 2.1), waffle images were used to obtain a precise measurement of the position of the star center for each frame, also taking into account the detector's dithering positions.

In the case of the non-coronagraphic images no waffle or PSF reference images were taken. We therefore used one of the images in the sequence as reference in order to be able to apply the DC data reduction procedure. The resulting data cube had to be then manually registered to ensure an accurate centering. For both epochs, after the preprocessing of each frame the speckle pattern subtraction was finally performed using both the PCA (Soummer et al. 2012; Amara & Quanz 2012) and the TLOCI (Marois et al. 2014) algorithms, combined with the the ADI technique. Figure 3 shows the achieved performances, in terms of magnitude and minimum companion mass, for both epochs.

### 2.3. IRDIS Long Slit Spectroscopy data

The LSS mode of IRDIS allows to obtain both medium ( $R\sim 350$ ) and low resolution spectra ( $R\sim 50$ ). For this study we only used the medium resolution spectrum, which not only allows the spec-

tral classification for the sub-stellar companion, but also provides information on key diagnostics such as e.g., the  $K_1$  and  $Nar$  lines that are identifiable with this resolving power.

The LSS data was analysed using the SILSS pipeline (Vigan 2016), which has been developed specifically to analyse IRDIS LSS data. The pipeline combines the standard ESO pipeline with custom IDL routines to process the raw data into a final extracted spectrum for the companion. After creating the static calibrations (background, flat field, wavelength calibration), the pipeline calibrates the science data and corrects for the bad pixels. It also corrects for a known issue of the MRS data, which produces a variation of the PSF position with wavelength because of a slight tilt ( $\sim 1$  degree) of the grism in its mount. To correct for this effect, the pipeline measures the position of the off-axis PSF in the science data as a function of wavelength, and shifts the data in each spectral channel by the amount necessary to compensate for the chromatic shift. All individual frames are calibrated independently for the two IRDIS fields. No speckle subtraction has been applied given the negligible flux of the central star at the separation of the sub-stellar companion.

Extraction and wavelength calibration of the 1D spectrum for the star, the companion and the early-type standard have been performed using *IRAF*<sup>1</sup> tasks. We have tested two different extraction procedures, one which uses a fixed window extraction of 6 pixels and another one which uses a window size which is function of  $\lambda / D$  (where  $D$  is the telescope diameter). The latter results in windows of roughly 3 pixels at  $0.9 \mu\text{m}$  and 7 pixels at  $1.8 \mu\text{m}$ . As the spectra provided by the two extraction methods appear to be in good agreement, we decided to keep the standard extraction (without pixel weighting) with a fixed width of 6 pixels, as it ensures higher signal-to-noise ratios (SNR, especially in the blue part). The SNR is  $\sim 15$  at  $1.3 \mu\text{m}$ .

As mentioned in Section 2, an early type star (The A3IV star HD 77281) was observed as part of the LSS observing sequence to obtain a more accurate wavelength solution.

The spectrum of HD 77281 was also used to correct the spectra of HD 284149 for the contamination of telluric lines, using the *IRAF* task *telluric*. This routine allows to account for small difference in the line intensity as well as possible wavelength shifts between the spectra of the science target and the template star.

The contrast spectrum of the companion was obtained by dividing by the spectrum of the primary extracted in an aperture of the same width. Then, in order to perform a comparison with a library of spectra and theoretical models, we calculated the flux spectrum of the brown dwarf by multiplying the contrast spectrum by the flux spectrum of the primary. To calculate the flux spectrum of HD 284149 we used the models by Brott & Hauschildt (2005)<sup>2</sup>, with  $B-V$  values retrieved from Nomad (Zacharias et al. 2004), 2MASS (Skrutskie et al. 2006) and WISE photometric information (Wright et al. 2010) and adopted a reddening of  $E(B-V)=0.08$  mag (see e.g., Bonavita et al. 2014). We verified the reddening value from Bonavita et al. (2014) using the IRSA tools available at [http://irsANSWER:ipac.caltech.edu/applications/DUST/](http://irsANSWER.ipac.caltech.edu/applications/DUST/) which yield a values of  $E(B-V) = 0.25-0.30$ . Considering that these values refer to total reddening within the Milky Way and considering the galac-

<sup>1</sup> IRAF is the Image Reduction and Analysis Facility, a general purpose software system for the reduction and analysis of astronomical data. IRAF is written and supported by National Optical Astronomy Observatories

<sup>2</sup> available for download at <ftp://ftp.hs.uni-hamburg.de/pub/outgoing/phoenix/GAIA>

Table 1: Main characteristics of the setup of the SPHERE observations of the HD 284149 system

Date	Mode	Filter	Coronagraph	Total Integration Time (s)		Total Field of View Rotation (deg)
				IFS	IRDIS	
2015-02-03	IRDIS_LSS	YJH	Y	–	180	–
2015-10-25	IRDIFS	H23	Y	256	256	22.13
2015-11-27	IRDIFS_EXT	K12	N	82.5	56.08	29.71

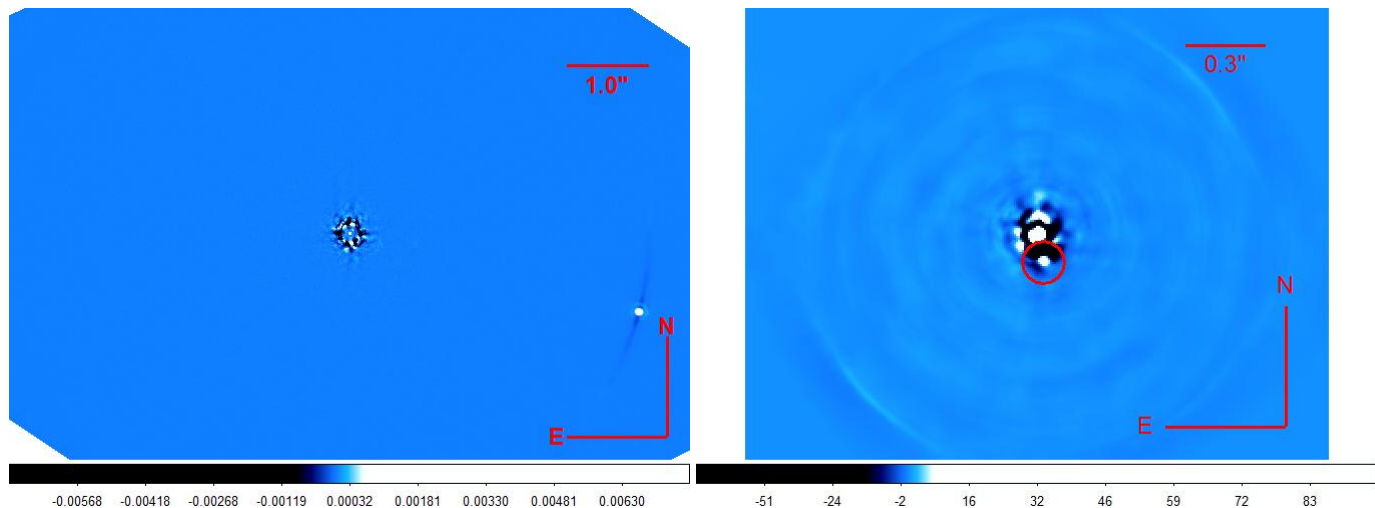


Fig. 1: Non coronagraphic IRDIFS\_EXT images of the HD 284149 system acquired on November 27th 2015. **Left:** Full-frame, TLOCI post-processed IRDIS image. The newly discovered close stellar companion HD 284149 B (see Section 4.1) is only barely visible in the IRDIS images. The known brown dwarf companion HD 284149 b (see e.g. Section 4.2) is clearly visible in the lower right corner. **Right:** PCA post-processed IFS image. The red circle marks the position of HD 284149 B.

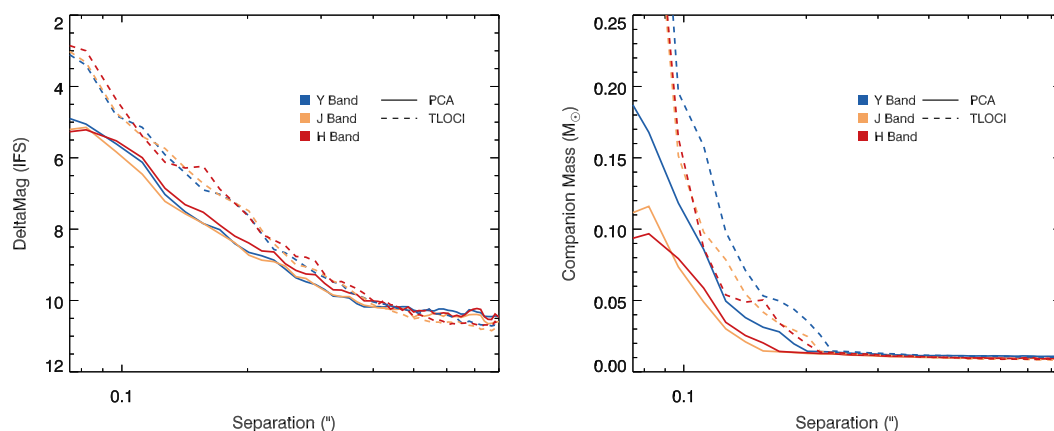


Fig. 2: IFS detection limits achieved during the non-coronagraphic observations of HD 284149 in terms of  $\Delta\text{mag}$  (left panel) and minimum companion mass (right panel) vs separation. The mass limits are evaluated using the COND models by Baraffe et al. (2003) and assuming an age of 35 Myrs. The different colours show the limits for the *Y*, *J* and *H* IFS filters respectively. The dashed line shows the limits evaluated using the images processed using the TLOCI method for speckle suppression (Marois et al. 2014), while the solid lines show the ones obtained using the images reduced using the PCA algorithm (Soummer et al. 2012; Amara & Quanz 2012).

tic position of HD 284149, we concluded that these values are fully compatible with the adopted ones.

The best spectral fit is obtained assuming  $T_{\text{eff}}=6000\text{K}$  and  $\log g=4.5$  dex (with  $g$  in  $\text{cm s}^{-2}$ ), in very good agreement with literature estimates in the ranges  $T_{\text{eff}}=5876\text{--}6184$  K (Bailer-Jones 2011),  $T_{\text{eff}}=5931\text{K}$  (McDonald et al. 2012), and  $T_{\text{eff}}=5970\text{--}6100$  K (Bonavita et al. 2014).

### 3. Stellar Properties

A comprehensive analysis of various stellar properties and age indicators of the star was performed in Bonavita et al. (2014), yielding an estimate of  $25_{-10}^{+25}$  Myr. The availability of Gaia DR1 data sets (Gaia Collaboration et al. 2016a) as well as the recent revision of the ages of several young moving groups used as reference (Bell et al. 2015) calls for a reassessment of the stellar properties. We also exploit photometric time series to refine the

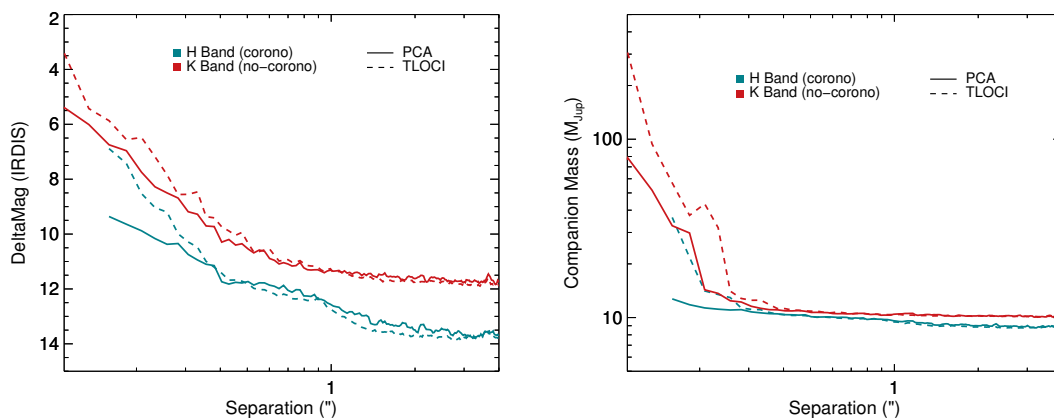


Fig. 3: IRDIS detection limits achieved during the observations of HD 284149 in terms of  $\Delta\text{mag}$  (left panel) and minimum companion mass (right panel) vs separation. The mass limits are evaluated using the BT-Settl models by Allard et al. (2012) and assuming an age of 35 Myrs. The blue and red curves show the limits achieved for the coronagraphic and non coronagraphic images, respectively. The dashed line shows the limits evaluated using the images processed using the TLOCI method for speckle suppression (Marois et al. 2014), while the solid lines show the ones obtained using the images reduced using the PCA algorithm (Soummer et al. 2012; Amara & Quanz 2012).

rotation period determination and better characterise the photometric variability of the star.

### 3.1. Stellar properties from Gaia-DR1

Gaia-DR1 yields a trigonometric parallax of  $8.51 \pm 0.27$  mas for HD 284149. Even after inclusion of a systematic error of 0.30 mas, as recommended by Gaia Collaboration et al. (2016b), this represents a substantial improvement with respect to the value by van Leeuwen (2007) ( $9.24 \pm 1.58$  mas). The resulting value of the distance of HD 284149 is then  $117.50 \pm 5.5$  pc. The slightly larger intrinsic luminosity makes the star well detached from the ZAMS, allowing a reliable age estimate based on comparison with pre-main sequence evolutionary models, while previous attempts were inconclusive due to the error on parallax. Figure 4 represents an update of Figure 2b by Bonavita et al. (2014).

Ages younger than 15 Myr and older than 30 Myr appear unlikely. On the other hand, plotting the members of  $\beta$  Pic moving group and Tuc-Hor association from Pecaat & Mamajek (2013) seems to suggest that, while the most probable locus of Tuc-Hor members is at fainter magnitudes, some individual members are in similar position to HD 284149 in the HR diagram. Nevertheless, an age as young as  $\beta$  Pic moving group is favoured by this comparison. A dedicated analysis aimed at obtaining a more precise estimate of the age is presented in Section 3.3.

### 3.2. Photometric analysis and rotation period

We retrieved a photometric time series collected during the 2004 and 2006 observation seasons from the SuperWASP public archive (Wide Angle Search for Planets Butters et al. 2010). It consists of 3892 V-band measurements with an average photometric precision  $\sigma = 0.006$  mag. After the removal of outliers from the time series applying a moving boxcar filter with  $3\sigma$  threshold, we averaged consecutive data collected within 30 minutes, and finally we were left with 652 averaged magnitude values for the subsequent analysis.

We used the Lomb-Scargle periodogram analysis (LS Scargle 1982), with the prescription of Horne & Baliunas (1986), on the SuperWASP time series to search for the rotation period of

HD 284149 (see Figure 5). From the computed stellar radius ( $R \sim 1.36 R_{\odot}$ , see below) and the measured projected rotational velocity, the rotation period is expected to be shorter than about 2 days. We therefore carried out our period search in the period range 0.1–10d.

In the left panel of Figure 5, we plot the LS periodogram as black solid line, whereas the red dotted line is the spectral window function. We detected a number of highly significant power peaks with False Alarm Probability (FAP)  $< 0.1\%$ . The FAP is the probability that a power peak of that height simply arises from Gaussian noise in the data, and was estimated using a Monte-Carlo method, i.e., by generating 1000 artificial light curves obtained from the real one, keeping the date but permuting the magnitude values according to their uncertainty. The most significant peak is at  $P = 1.051 \pm 0.005$  d (with a FAP of  $\sim 10^{-6}$ ), which we assume to represent the stellar rotation period. This value is similar, although formally significantly different, to the rotation period  $P = 1.073$  d previously measured by Grankin et al. (2007) and inferred from data collected at the Mt. Maidanak Observatory. All the other significant power peaks at shorter periods in the LS periodogram are harmonics, arising from the one-day sampling interval imposed by the rotation of the Earth and the fixed longitude of the observation site. We note a second highly significant power peak at  $P = 1.074$  d, almost identical to the literature value. Such a period may arise from the presence of two spot groups at different average latitudes on a differentially rotating star. In this case, HD 284149 would have a lower limit of the surface differential rotation of  $\sim 2\%$ . However, when we fold the light curve with the rotation period, as shown in the right panel of Figure 5, we note that in the 2006 observation season the light curve undergoes a rapid change of the phase of minimum ( $\Delta\phi \approx 0.25$ ) and of the peak-to-peak amplitude (from  $\Delta V = 0.02$  mag to  $\Delta V = 0.04$  mag), suggesting a rapid reconfiguration of the active regions. Indeed, it is interesting to consider the possible effect of active regions growth and decay (ARGD) on spurious variations of the photometric period. Dobson et al. (1990) and Donahue & Baliunas (1992) have proposed a method, the so-called pooled variance analysis, to estimate the time scale of evolution of an active region. This method is based on the analysis of the variance in photometric time series

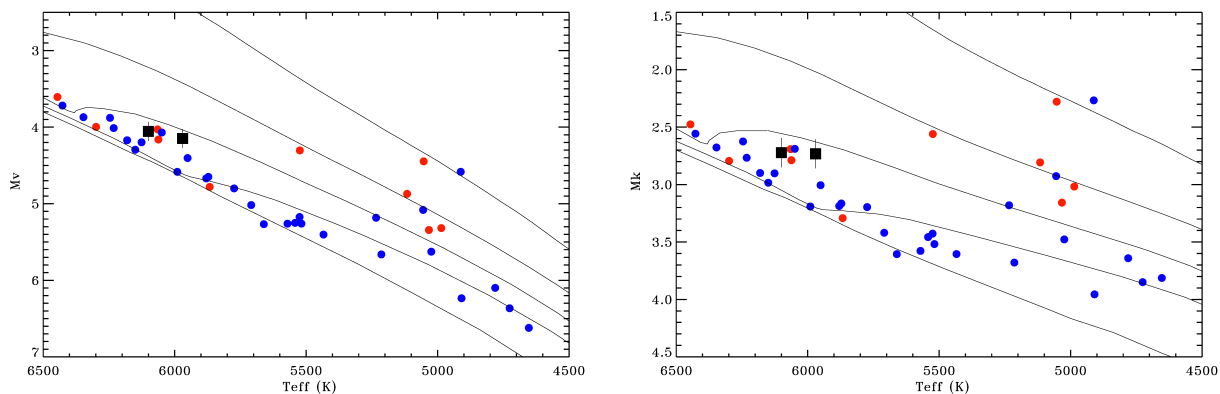


Fig. 4: Position of HD 284149 (black squares) on the H-R diagram for the temperatures corresponding to F8 and G1 spectral classification (see Bonavita et al. 2014, for V and Ks band magnitudes (upper and lower panels, respectively)). Over plotted are the 5, 12, 20, 30, and 70 Myr isochrones of solar metallicity from Bressan et al. (2012) and the members of the  $\beta$  Pic moving group (red circles) and Tuc-Hor association (blue circles) with available trigonometric parallax from the list of Pecaut & Mamajek (2013).

over different time scales. The variance profile of HD 284149 is plotted in the left panel of Figure 6. We note that the variance monotonically increases and does not show any plateau at time scales longer than the rotation period, which is marked with a vertical dotted line in Figure 6. This behaviour is characteristic of ‘activity-dominated’ stars (see Messina & Guinan 2003), that is of stars whose active regions are not stable, but evolve with the same time scale as the stellar rotation. This would explain the large phase scatter, despite the high photometric precision, the presence of the two close peaks in the periodogram, the family of lower power peaks clustering around the two major peaks, and the difference with respect to the literature value. We conclude that secondary peaks are due to the ARGD rather than to surface differential rotation.

It is interesting to see that combining the available V-band photometry from Hipparcos (to which we applied a correction of -0.137 mag to transform into the Johnson system), from ASAS (All Sky Automated Survey, see Pojmanski 1997), Grankin et al. (2007) and SuperWASP (to which, to be consistent with ASAS data we applied a correction of -0.23 mag) HD 284149 exhibits a long-term brightness variation which likely is related to a star spot cycle with an amplitude of  $\Delta V \gtrsim 0.2$  mag (see Figure 6).

Using the brightest visual magnitude  $V = 9.55$  mag inferred from the ASAS time series, a reddening  $E(B-V) = 0.08$  mag (Bonavita et al. 2014), distance  $d = 117.50 \pm 5.5$  pc from Gaia-DR1, bolometric correction  $BC_V = -0.07 \pm 0.02$  (Pecaut & Mamajek 2013), we derive the luminosity  $L = 2.20 \pm 0.45 L_\odot$ . Using the measured effective temperatures in the range  $T = 5970\text{--}6100$  K (Bonavita et al. 2014), we derive an average stellar radius  $R = 1.36 \pm 0.33 R_\odot$ . Combining rotation period and projected rotational velocity  $v \sin i = 27.0 \pm 1.9 \text{ km s}^{-1}$  (Bonavita et al. 2014), we derive the inclination of the rotation axis  $i = 25 \pm 5^\circ$ .

### 3.3. Stellar age

A comparison of the rotation period of HD 284149 with the distribution of rotation periods of associations of known age allows us to constrain its age. We find that the rotation period  $P = 1.051$  d well fits into the period distribution of Tucana/Horologium, Carina, and Columba that have an age originally quoted to be 30 Myr but recently revised to 42–45 Myr (Bell et al. 2015). On the other hand, HD 284149 rotates slightly slower than most of the equal-mass association members of the

$25 \pm 3$  Myr  $\beta$  Pic Associations (e.g. Messina et al. 2016) with just a couple of confirmed members in the same region in a color-period diagram (Messina et al. 2017, submitted). Finally HD 284149 rotates significantly faster than the equal-mass members of Pleiades.

Therefore, on the basis of rotational properties, our target seems to have an age close to that of Tuc-Hor, but possibly as young as  $\beta$  Pic moving group members. The Lithium EW is compatible with both  $\beta$  Pic moving group and Tuc-Hor moving group members (Bonavita et al. 2014) and clearly rules out ages as old as Pleiades or AB Dor MG. The isochrone fitting<sup>3</sup> indicates an age similar to that of  $\beta$  Pic moving group members, although when plotting Tuc-Hor members on CMD a couple of individual late F - early G members are as bright as HD 284149. Therefore, we can conclude that HD 284149 has an age between 20 and 45 Myr, with a most likely value of 35 Myr.

A finer age assessment is limited by the intrinsic spread of the various indicators at fixed age (as retrieved from moving group members). Improvements could arise from analysis of additional coeval stars coming with HD 284149. Daemgen et al. (2015) found that this star, together with several other objects known as bona-fide Taurus members, has similar space position and kinematics to those of the Taurus star forming region, but also shows evidence of a distinctly older age. They proposed an age of about 20 Myr for what is now called the *Taurus-Ext Association* (see Appendix A in Daemgen et al. 2015, and references therein) from comparison of Lithium EW with that of the oldest Sco-Cen groups (Pecaut & Mamajek 2016). Such proposed age for the group is at the young edge of our age range.

Finally, we mention that the low mass companion detected with SPHERE (see Sect. 4.1) has negligible impact on the age indicators, due to its faintness with respect to the central star, apart from some minor effects on kinematics.

<sup>3</sup> Figure 4 is based on comparison with Bressan et al. (2012) models. The choice of adopted models does not affect significantly the results. Indeed we extended the comparison presented in Desidera et al. (2015) to the recently published models by Choi et al. (2016), finding good agreement for the masses and ages of interest for this study.

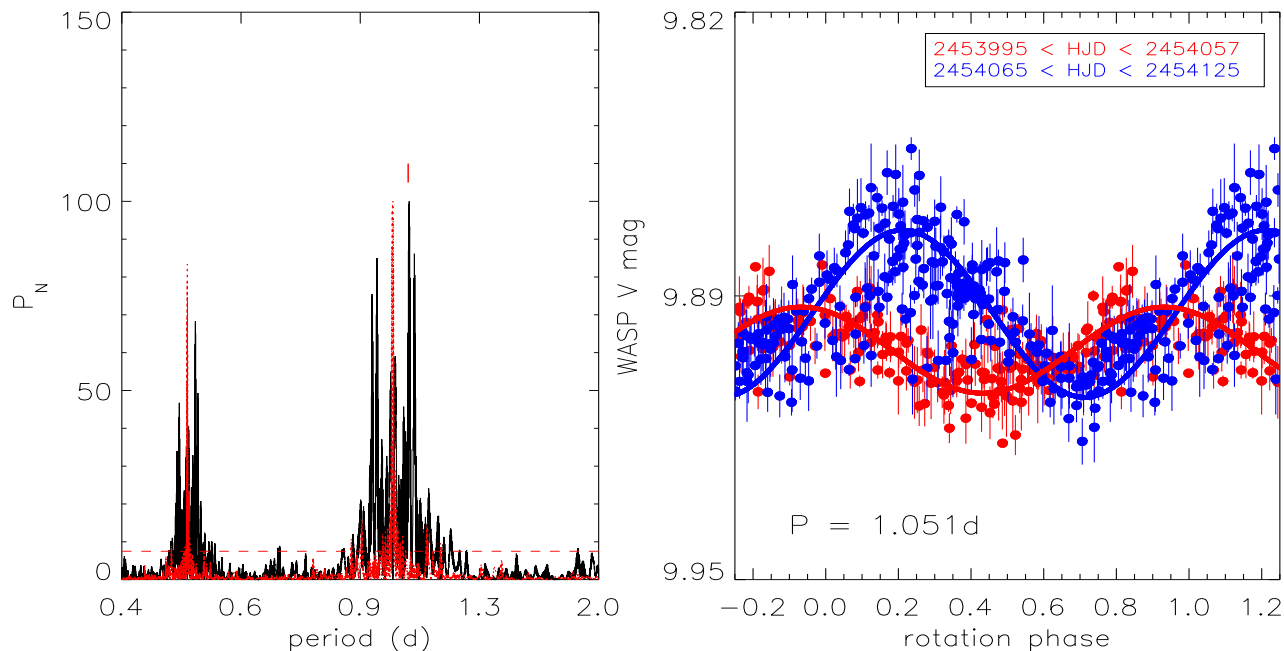


Fig. 5: Left panel: Lomb-Scargle periodogram of HD 284149 of the SuperWASP V magnitude time series collected in 2004 and 2006. The normalised power ( $P_N$ ) (black solid line) is plotted versus period. The red dotted line represents the spectral window function, whereas the red horizontal dashed line indicates the power level corresponding to a FAP = 0.1%. Right panel: SuperWASP V magnitudes of HD 284149 collected in 2006 and phased with the photometric rotation period  $P = 1.051 \pm 0.005$  days. Solid lines are the sinusoidal fits to phased data collected in the date range 2453995 < HJD < 2454057 (red) and in 2454065 < HJD < 2454125 (blue).

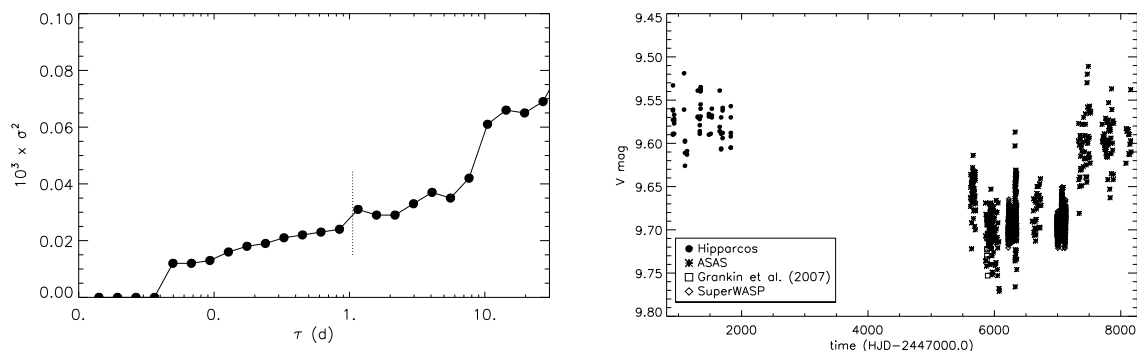


Fig. 6: Left Panel: Pooled variance profile of HD 284149 computed on the SuperWASP V-mag time series. Right Panel: Long-term V-band magnitude time series of HD 284149.

## 4. Results

### 4.1. Discovery of a close low-mass stellar companion

The non-coronagraphic IFS data of HD 284149 revealed a stellar companion at very small separation from the star. The companion (hereafter HD 284149B B) was visible but partially obscured by the coronagraph in the previous epoch, which then justified the choice for the non-coronagraphic mode for the following observations. HD 284149 B was successfully retrieved in both the IFS and the IRDIS non-coronagraphic images, both reduced using the PCA algorithm for speckle suppression. The right panel of Figure 1 shows the processed IFS images, and the correspond-

ing S/N map is shown in Figure 7. In both figures the position of HD 284149 B is marked by a red circle.

#### 4.1.1. Astrometry and photometry

Table 2 shows the values of IRDIS and IFS astrometry and photometry for HD 284149 B. The IFS photometry for HD 284149 B in the  $Y$ ,  $J$  and  $H$  band was obtained considering the median contrast in the wavelength range between 0.95 and 1.15  $\mu\text{m}$  for the  $Y$  band, between 1.15 and 1.35  $\mu\text{m}$  for the  $J$  band and between 1.35 and 1.65  $\mu\text{m}$  for the  $H$  band. The non-coronagraphic IRDIS images provided the contrast in the  $K1$  and

Table 2: IFS and IRDIS astrometry of HD 284149 B from the non-coronagraphic data obtained in November 2015.

filter	Separation		PA ( $^{\circ}$ )	$\Delta$ mag	Mass ( $M_{\odot}$ )
	(mas)	(au)			
<i>Y</i>	$90.02 \pm 1.32$	$10.58 \pm 0.15$	$195.19 \pm 1.86$	$4.54 \pm 0.13$	$0.23 \pm 0.02$
<i>J</i>	$90.73 \pm 1.22$	$10.66 \pm 0.15$	$194.99 \pm 1.66$	$4.57 \pm 0.11$	$0.17 \pm 0.02$
<i>H</i>	$94.18 \pm 1.16$	$11.07 \pm 0.16$	$195.03 \pm 1.47$	$4.87 \pm 0.23$	$0.12 \pm 0.01$
<i>K1</i>	$80.16 \pm 18.57$	$9.42 \pm 0.66$	$187.53 \pm 67.03$	$4.07 \pm 0.24$	$0.19 \pm 0.02$
<i>K2</i>	$81.72 \pm 18.27$	$9.60 \pm 0.66$	$193.22 \pm 34.00$	$3.79 \pm 0.21$	$0.20 \pm 0.02$
Adopted values					
	$91.78 \pm 2.16$	$10.71 \pm 0.34$	$195.06 \pm 0.16$	–	$0.16 \pm 0.04$

**Notes.** A true north position of  $-1.7470 \pm 0.0048^{\circ}$  and pixel scale of  $7.46 \pm 0.02$  mas/pixel and  $12.255 \pm 0.009$  mas/pixel, for IFS and IRDIS respectively (see Maire et al. 2016b, for details) were used. The value of the separation in AU was obtained using the value of the parallax of the star provided by the Gaia satellite (Gaia Collaboration et al. 2016b). The values of the masses are derived using the COND Models by Baraffe et al. (2003) and taking into account both the uncertainties on the photometry and on the age value. The uncertainties listed take into account all the possible sources of errors. Note that in the case of the astrometry, the dominant source of error is the uncertainty on the centering of the star, whether the error on the mass is dominated by the uncertainty on the age estimate.

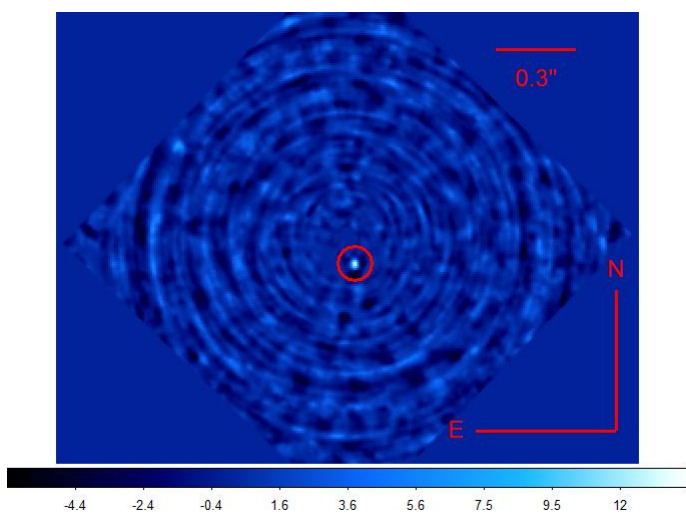


Fig. 7: Signal to noise map obtained for the non-coronagraphic IFS data of HD 284149. The position of the newly discovered low-mass stellar companion HD 284149 B is marked by a red circle. The peak of the SNR at the companion position is of  $\sim 15$ .

*K2* bands instead. From these values, using the COND models by Bate et al. (2003) and assuming an age of  $35^{+10}_{-15}$  Myr (see Section 3.3), we were able to estimate the mass of the companion for each spectral band (also reported in Table 2).

For each band we also obtained an independent value of the companion separation and position angle. The total uncertainty listed above takes into account all the possible sources of error but the final error bars are mainly dominated by the uncertainty on the centering of the star. We derived a mass of  $0.16 \pm 0.04 M_{\odot}$  and a separation of  $91.8 \pm 2.2$  mas for HD 284149 B, combining the measurements from the different bands (see Table 2 for details).

Figure 8 shows the location of HD 284149 B on a K-band based colour-magnitude diagrams (CMD). The positions of M, L and T field dwarfs and of young known companions are shown for comparison. Details on how the diagrams are generated are given in Mesa et al. (2016b) and Samland et al. (2017). The field dwarf spectra used to generate the synthetic photometry are taken from the SpeXPrism library (Burgasser 2014); Leggett et al. (2000), and from Schneider et al. (2015). We used for the most part distances reported in Harrington & Dahn (1980),

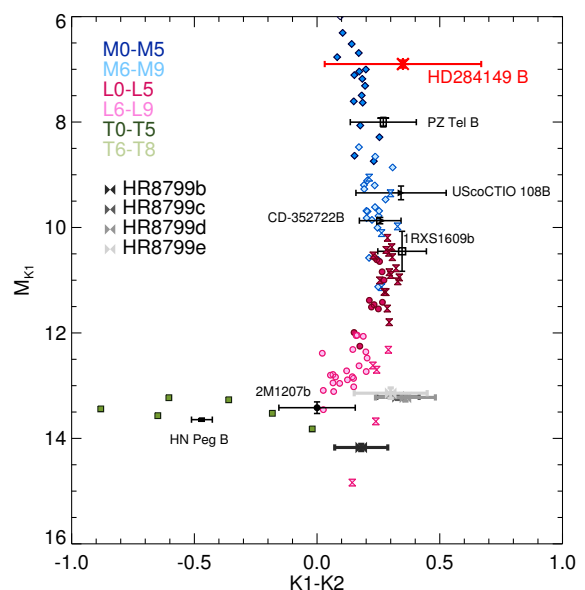


Fig. 8: Colour magnitude diagram showing the position of HD 284149 B (red bow tie) relative to that of M, L and T field dwarfs and of young known companions, based on the K1-K2 photometry from the non-coronagraphic IRDIS data (see text for details).

Kirkpatrick et al. (2000), Jenkins et al. (2009), Faherty et al. (2012), and Dupuy & Kraus (2013). We overlaid the photometry of young and/or dusty free-floating objects. Their absolute photometry was synthesised from their spectra (Liu et al. 2013; Mace et al. 2013; Allers & Liu 2013; Gizis et al. 2015) and the corresponding parallaxes (Kirkpatrick et al. 2011; Faherty et al. 2012; Zapatero Osorio et al. 2014; Liu et al. 2016). We added the photometry of companions using the spectra and distances reported in Wahhaj et al. (2011a); Gauza et al. (2015b); Stone et al. (2016b); De Rosa et al. (2014); Lachapelle et al. (2015); Bailey et al. (2014b); Rajan et al. (2017); Bonnefoy et al. (2014); Patience et al. (2010); Lafrenière et al. (2010).

The position of HD 284149 B, between the lower end of the M0-M5 sequence and the upper end of the M6-M9 sequence, seems to suggest a mid-M spectral type.

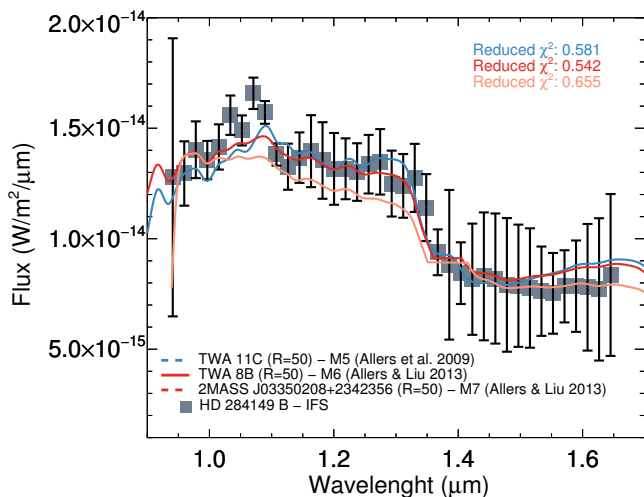


Fig. 9: Comparison of the spectrum of HD 284149 B (grey squares) with the spectra of TWA8 B (Allers et al. 2009), TWA 11 C and 2MASS J03350208+2342356 (Allers & Liu 2013). The values of the reduced  $\chi^2$  obtained for the fit are shown in the top right corner. TWA8 B (red curve) provides the best fit.

#### 4.1.2. Spectral characterisation

Exploiting the 39 IFS wavelengths we were able to extract a low resolution spectrum for the HD 284149 B. However, it is known that PCA tends to introduce biases on photometric data. Therefore we decided to use an alternative approach to extract the spectrum. We calculated a median data cube from the initial data set composed by all the calibrated data cubes after rotating each of them by the proper rotation angle previously calculated in such a way that the whole data set is perfectly aligned. For each image of the median data cube we then calculated the stellar profile by estimating the median of all the pixels at the same separation from the central star which was then subtracted from the original image. On each wavelength frame of the resulting data cube we applied a three pixels radius aperture photometry. For each wavelength the resulting photometry was then normalised to the flux of the correspondent wavelength of the central star. This approach also has the advantage of allowing to correct for the effect of the telluric lines as they affect both the primary and the secondary at the same way.

The extracted spectrum was then fitted with spectra of known objects from two different libraries: the Montreal Spectral Library<sup>4</sup> and the one from Allers & Liu (2013). The best fit, as shown in Figure 9, was obtained with the spectrum of TWA8 B (Allers et al. 2009), classified by Allers & Liu (2013) as a very low-gravity object (VL-G), with an assigned spectral type of M6. The spectra of TWA 11 C and 2MASS J03350208+2342356, classified as M5 and M7 respectively (Allers & Liu 2013), are shown for comparison. We therefore conclude that the spectra of HD 284149 B is compatible with a spectral type of M6 $\pm$ 1 (No attempt was made to assign a gravity class to the object, given the limited resolution and signal to noise of the IFS spectra). This is in good agreement with the estimate obtained using the IRDIS photometry (see Section 4.1.1).

#### 4.1.3. Dynamical signatures of the close companion

The discovery of a stellar companion to HD 284149 comes as confirmation to several dynamical signatures hinting to its existence.

A radial velocity difference of 3 km s<sup>-1</sup> between the early measurement by Wichmann et al. (2000) and the recent sequence by Nguyen et al. (2012) was already noticed in Bonavita et al. (2014). Assuming a mass of  $\sim 0.167 M_{\odot}$  and a semi-major axis of 10.7 AU (equal to the projected separation), the expected RV semi-amplitude of the newly discovered companion is about 1.32 km s<sup>-1</sup> for an edge-on circular orbit. We therefore conclude that the newly discovered companion is likely to be responsible for the observed radial velocity difference. This opens the perspective for a determination of dynamical mass by coupling spectroscopic and imaging monitoring, which would be relevant given the young age of the system, as dynamical measurements of the mass are available only for few young binaries (see e.g. Dupuy et al. 2016).

An additional dynamical signature related to the presence of moderately close companions is the detection of significant differences in the proper motion of a star as measured at different epochs. Such systems were first identified as  $\Delta\mu$  binaries in the pioneering work by Makarov & Kaplan (2005), who exploited the difference between the short-term proper motion measured by Hipparcos (epoch 1991, baseline 3.25 yr) and the long-term (a century timescale) proper motion by the Tycho-2 catalogue. The release of Gaia-DR1 offers an additional opportunity to check for the detection of proper motion differences, providing proper motion measurements on a  $\sim 24$  yr baseline from the combination of Gaia-DR1 data with Hipparcos positions.

HD 284149 has no significant  $\Delta\mu$  in Makarov & Kaplan (2005) but a comparison of its Gaia and Tycho-2 proper motions yields  $\Delta\mu_{\alpha} = -3.32 \pm 1.01$  mas/yr and  $\Delta\mu_{\delta} = 0.08 \pm 1.00$  mas/yr. Significant proper motion difference is also seen between Gaia and UCAC4 measurements<sup>5</sup>, while Gaia and Hipparcos values do not differ significantly. Although HD 284149 wasn't selected for observation because of its proper motion discrepancies, its newly detected companion then represents an ideal candidate for a dynamical characterisation that takes advantage from the combination of astrometry and imaging data.

We therefore used the COPAINS (Code for Orbital Parametrization of Astrometrically Identified New Systems, Fontanive et al. private comm.) code to evaluate the characteristics of the possible companions compatible with the observed  $\Delta\mu$ . The code uses Eq. 1<sup>6</sup>, derived by Makarov & Kaplan (2005), to estimate the change in a star's proper motion induced by a given companion, for a range of possible masses and separations. A fine grid of mass and separation values is explored, and the expected  $\Delta\mu$  is evaluated and compared with the observed one. In order to properly take into account the projection effects, for each point on the mass-separation grid the code considers 10<sup>6</sup> possible orbital configurations, with eccentricities drawn from either a uniform or Gaussian (see Bonavita et al. 2014, and references therein for details) distribution.

<sup>5</sup> As our results could be highly affected by systematic errors which could arise from an improper estimation of the proper motion error bars, we decided to consider only the value of  $\Delta\mu$  obtained using Tycho-2 for our analysis.

<sup>6</sup> In Eq. 1  $M_2$  is the mass of the secondary,  $M_{Tot}$  is the total mass of the binary,  $a$  is the semi-major axis in AU,  $\Pi$  is the parallax of the system in mas, and  $R_0$  takes into account the orbital phase so that  $R_0 = \left( \frac{1+e \cos E}{1-e \cos E} \right)^{1/2}$  where  $e$  is the orbital eccentricity and  $E$  is the eccentric anomaly

<sup>4</sup> <https://jgagneastro.wordpress.com/the-montreal-spectral-library>

Figure 10 shows the results obtained for the two cases. In both panels the area enclosed by the two dashed lines shows the position on the mass-separation space of the companions that would cause a  $\Delta\mu$  within one sigma from the observed one. Regardless of the assumption on the eccentricity distribution, the observed mass and separation of HD 284149 B (see Table 2) seems to be compatible with the observed trend.

Finally, the mass distribution for companions at the observed separation of HD 284149 B and compatible with the observed trend is shown in Figure 11. For the flat and Gaussian eccentricity priors, the posterior Mass distribution peaks at  $0.20^{+0.12}_{-0.04} M_{\odot}$  and  $0.23^{+0.07}_{-0.09} M_{\odot}$  respectively, and is therefore compatible with the value obtained from the SPHERE photometry ( $0.16 \pm 0.04 M_{\odot}$  see Table 2).

$$\Delta\mu \leq \frac{2\pi IR_0 M_2}{\sqrt{a M_{Tot}}} \quad (1)$$

## 4.2. Characterisation of the known brown dwarf companion

### 4.2.1. IRDIS Astrometry

Precise relative astrometry for HD 284149 b was obtained from both the coronagraphic H2 and H3 images using the SHINE Special pipeline (Galicher et al. private comm.).

For the non-coronagraphic images we used PSF fitting with the *digiphot/allstar* routine in *IRAF*. For each individual exposure in the image cubes (400 exposures per filter), we measure the relative pixel position between the two point sources using an 80 pix-radius reference PSF composed from the unsaturated primary in all exposures per filter with the *iraf/digiphot* task *psf*. For efficiency, before applying *allstar*, we cut out 160×160 pixel regions around both the primary and the companion for every individual exposure (400 exposures total) and re-arrange these into two separate 20×20 star grids per filter. The final astrometry was reconstructed by reverse-applying the offsets of this mapping process. Measured pixel positions were transformed to separation and position angle by derotating with the sky rotation angle from the fits header and assuming a pixel scale of  $12.255 \pm 0.009 \text{ mas/pix}$  and a true north position of  $-1.70 \pm 0.10^\circ$  for the 2015-10-25 epoch and  $-1.747 \pm 0.048^\circ$  for the 2015-11-29 epoch (see Maire et al. 2016a). The values obtained for both cases are reported in Table 3.

The combined astrometry from the two epochs is  $\text{sep}=3669.14 \pm 0.91 \text{ mas}$  and  $\text{PA}=255.00 \pm 0.01^\circ$  taking into account all the random and systematic uncertainties. Adopting the new distance to the system from Gaia, we obtain a value of the projected separation of HD 284149 b of  $431.2 \pm 2.9 \text{ AU}$ .

Figure 12 shows the updated common proper motion plot.

We did not attempt to constrain the orbital properties of the brown dwarf companion due to the insufficient time baseline of the observations (4 yrs compared to an expected period of over 6000 yrs for a pole-on circular orbit) and because of the unknown orbit of the close stellar companion, which could bias the derived orbital properties if not taken into account (Pearce et al. 2014).

### 4.2.2. IRDIS photometry

Table 3 shows the values of the relative photometry of HD 284149 b. The values for the H2 and H3 bands were obtained using the coronagraphic data taken in October 2015, while we derived the K1 and K2 photometry from the non-coronagraphic

observations. The values of the masses were obtained using the BT-Settl models by Allard et al. (2012) and taking into account both the uncertainties on the photometry and on the age, the latter being once again the dominating source of error. Combining these results we obtain for HD 284149 b a mass of  $26 \pm 3 M_{Jup}$ .

Finally, we used the IRDIS photometry to study the position of HD 284149 b in a color-magnitude diagram (CMD), compared with those of known MLTY field dwarfs, brown dwarfs and known directly imaged young companions (See Section 4.1.1 for details on the construction of the plots).

As shown in Figure 13, HD 284149 b (red bow tie) falls on the sequence of M6-M9 field dwarfs in both the K band and H band diagrams, and it is nicely bracketed by UScoCTIO 108 (an M9.5, see Béjar et al. 2008, for details) and CD-352722 B (an L1±1, see Wahhaj et al. 2011b).

### 4.2.3. Spectral characterisation

The very high quality of the spectra obtained with the LSS mode of IRDIS (see Section 2.3) allows us to put strong constraints on the spectral type of HD 284149 b, through the comparison with available libraries of spectra of similar objects.

We first compared it with to the medium-resolution ( $R \approx 2000$ , SXD mode) SpeX spectral library by Allers & Liu (2013), which includes observed spectra for M, L, and T dwarfs (both young and old). In order to perform the comparison, those spectra were downgraded to our resolution of  $R \approx 350$ . This was done by convolution with a Gaussian function of the appropriate full width half maximum.

The result of the  $\chi^2$  procedure that we have carried out in order to obtain the best fit is shown in Figure 14. The best fit is obtained using the spectra of LP 944-20, classified as M9 $\beta$  (Allers & Liu 2013). The plot clearly shows how, while the global shape of the pseudo-continuum is well represented by this spectral type, the gravity sensitive features (e.g., Na I, K I) of our target are significantly weaker. This suggests that HD 284149 b has a lower gravity, thus pointing to a younger age with respect to the template spectrum.

To further investigate this point, we also carried out a spectral comparison with template spectra for young brown dwarfs from the Montreal Spectral Library<sup>7</sup> (see Figure 15 and 16).

The best fitting spectra in this case is the one of 2MASS J0953212-101420 (Gagné et al. 2015, top panels of Figure 15), a M9  $\beta$ . However, although the pseudo continuum is very well reproduced, again the spectral features are much weaker in our target. Conversely, the M9  $\gamma$  template provides a very good fit of the spectral lines (see lower panels of Figure 15), despite the fact that 2MASS J04493288+1607226 (Gagné et al. 2015) is not a perfect match of the global continuum.

Thus, we can conclude that HD 284149 b has a spectral type of M9 $\gamma$ , the Greek letter pointing to a low surface gravity, hence to a young age (see Kirkpatrick 2005).

According to previous estimates obtained using NIR photometry, HD 284149 b was expected to have a spectral type between M8 and L1 (see Bonavita et al. 2014). As a final check we therefore compared our spectra with the M8 and L0/L1 spectra from the Montreal Spectral Library. Figure 16 shows an example of such comparison, where only one example for each spectral type is plotted (blue solid line), together with our data (black solid line). As clearly neither spectral type provide a good

<sup>7</sup> available at <https://jgagneastro.wordpress.com/the-montreal-spectral-library/>, see e.g., Gagné et al. (2015)

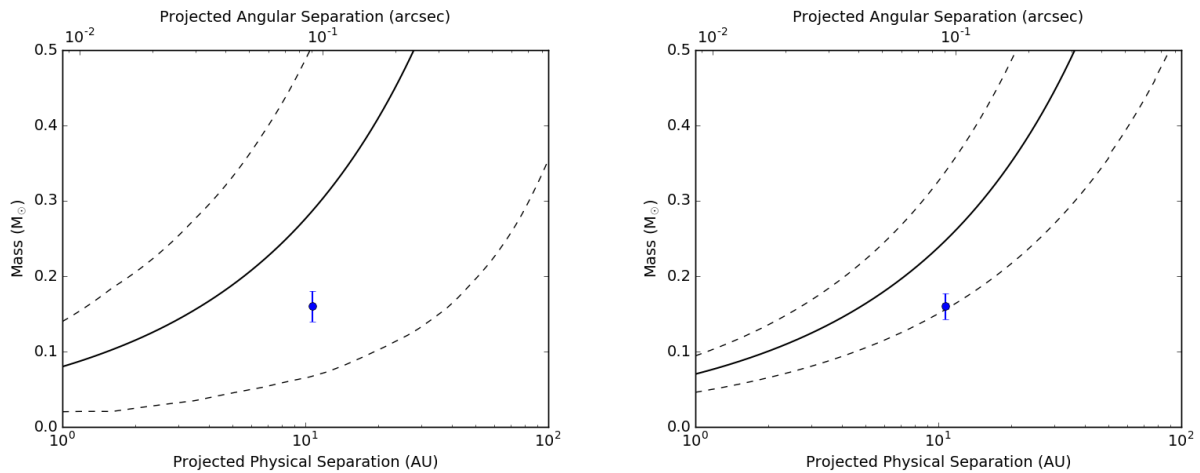


Fig. 10: Estimate of the mass and separation of the companions compatible with the observed  $\Delta\mu$ , assuming an orbit with an eccentricity randomly drawn from a flat (left panel) or Gaussian (right panel) distribution. The blue dot indicates the position of the detected companion.

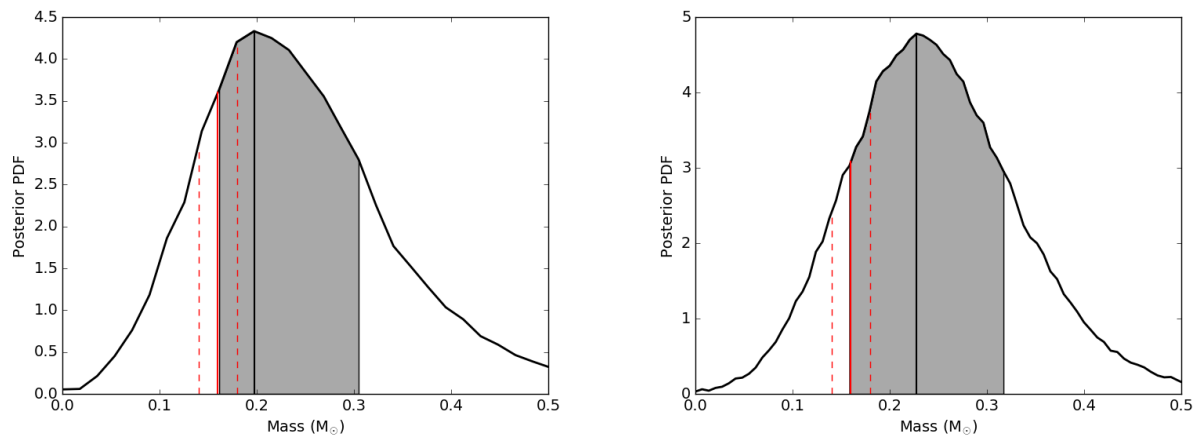


Fig. 11: Mass distribution of the companions compatible with the observed  $\Delta\mu$ , assuming a semi-major axis compatible with the observed projected separation of HD 284149 B, and an eccentricity randomly drawn from a flat (left panel) or Gaussian (right panel) distribution. The black solid line shows the position of the most likely value and the shaded area highlights the region within a 1 sigma confidence level. The red solid line marks the value of the mass of HD 284149 B (see Table 2)

Table 3: IRDIS Relative astrometry of HD 284149 b

filter	sep (mas)	sep (AU)	PA ( $^{\circ}$ )
<i>H2</i>	$3668.58 \pm 1.68$	$431.06 \pm 5.75$	$255.01 \pm 0.01$
<i>H3</i>	$3669.03 \pm 1.33$	$431.11 \pm 5.92$	$255.02 \pm 0.01$
<i>K1</i>	$3670.03 \pm 2.7 \pm 0.01$	$431.23 \pm 5.89$	$254.82 \pm 0.01 \pm 0.05$
<i>K2</i>	$3670.14 \pm 2.7 \pm 0.01$	$431.24 \pm 5.88$	$254.83 \pm 0.01 \pm 0.05$
Adopted values	$3669.14 \pm 0.92$	$431.16 \pm 2.93$	$255.01 \pm 0.01$

**Notes.** Reported numbers for *K1* and *K2* bands are mean values and their random uncertainties (standard error of the mean). When a second uncertainty is reported, it refers to the systematic uncertainty of the pixel scale and True North correction, respectively (see Sect. 4.2.1). The values of the separation in AU were obtained using the new parallax measurement from the Gaia mission (Gaia Collaboration et al. 2016b).

match of our data, we therefore conclude that the spectral type of HD 284149 b should be  $M9 \pm 0.5$ .

It is noteworthy, in this context, that the gravity-sensitive spectral features of K I lines provide further support to our conclusion, as they also point towards a very low-gravity object

(the Na I line at  $1.14 \mu\text{m}$  could not be used because of the occurrence of cosmic rays on top of the feature). We measure  $\text{EW}(\text{K I})_{1.169} = 2.70 \text{ \AA}$  and  $\text{EW}(\text{K I})_{1.177} = 4.72 \text{ \AA}$ , which provide a very strong indication of reduced gravity, confirmed by the position of HD 284149 b on diagnostic plots by Allers & Liu

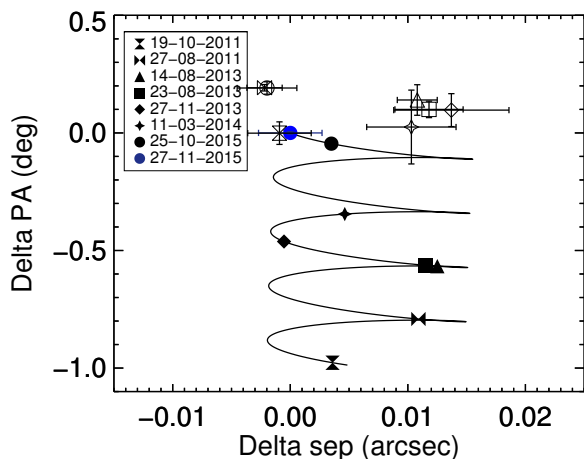


Fig. 12: Common proper motion analysis for HD 284149 b. The black solid line represents the motion of a background object. The filled symbols mark the positions of a background objects at the dates of the observations. The measured positions at the same dates are plotted with the corresponding open symbols. The blue filled circle marks the latest IRDIS\_EXT observation.

Table 4: IRDIS Relative photometry of HD 284149 b

Filter	$\Delta$ mag	Mass ( $M_{Jup}$ )
<i>H2</i>	$7.39 \pm 0.12$	$21.37 \pm 5.15$
<i>H3</i>	$7.17 \pm 0.12$	$20.11 \pm 3.76$
<i>K1</i>	$6.63 \pm 0.15$	$35.81 \pm 6.93$
<i>K2</i>	$6.34 \pm 0.16$	$34.94 \pm 7.09$
Adopted values	–	$26.28 \pm 2.93$

**Notes.** For the *K1* and *K2* bands, reported numbers are mean values and their random uncertainties (standard error of the mean). For all bands the values of the masses are derived using the BT-Settl Models by Allard et al. (2012) assuming an age of 35 Myrs (see Section 3.3). Although the error on the mass is dominated by the uncertainty on the age, the listed values also take into account the contribute of the uncertainties on the photometry.

(2013) (see their Figure 23). As a further check, we have calculated the gravity score for the brown dwarf, following prescriptions given in Allers & Liu (2013): by exploiting FeH bands, H-band continuum shape and K I lines we have obtained a four-digit score of 2212. Thus, our object can be classified as VL-G (i.e., very low gravity).

Note also that the very low-gravity we found for HD 284149 b allows an independent evidence on the system’s age, as M9y objects are consistent with ages younger than  $\sim 60$  Myr (Martin et al. 2017).

As a further independent confirmation of our estimate we have also calculated the  $H_2O$  spectral index, as defined in Allers & Liu (2013), which has been shown to be spectral-type sensitive and gravity insensitive (Allers et al. 2007; Allers & Liu 2013). HD 284149 b is found to have an H-index of 1.137 which implies a spectral type of  $M9 \pm 1$ , thus in very good agreement with the value coming from the visual inspection.

Finally, we have used the spectral type vs  $T_{\text{eff}}$  relationship as given by Filippazzo et al. (2015) and found a value of  $T_{\text{eff}} = 2395 \pm 113$  K. Our temperature estimate agrees very well

with previous findings by Bonavita et al. (2014), who reported  $T_{\text{eff}} = 2337^{+95}_{-182}$  K from the spectral type and the calibration by Pecaut & Mamajek (2013).

## 5. Discussion and conclusions

This paper presents a detailed characterisation of the HD 284149 ABb system<sup>8</sup>. We were able to refine the estimate of the spectral type of the known sub-stellar companion HD 284149 b (Bonavita et al. 2014), using high quality medium resolution spectra obtained with IRDIS in Long Slit Spectroscopy (LSS) Mode. Our results point toward an M9 spectral type and an effective temperature of 2300 K, with significant improvement with respect to the previous estimates.

A reassessment of the stellar properties was carried out, also taking advantage of the availability of Gaia measurement of parallax and proper motion, resulting in a distance of  $117.50 \pm 5.50$  pc and a stellar age of 35 Myr. As a consequence we were able to refine the previous estimates of both separation and mass of HD 284149 b ( $431.20 \pm 7.67$  AU and  $26 \pm 3 M_{Jup}$  respectively).

Finally, a close low-mass stellar companion (HD 284149 B  $\sim 0.16 M_{\odot}$  at  $\sim 0.1''$ ) was resolved in the IRDIFS non-coronagraphic images. Such companion is compatible with the radial velocity difference pointed out by Bonavita et al. (2014) as well as with the difference in proper motion between the Gaia and Tycho2 measurements. Therefore, there are good potential for dynamical mass determination for the HD 284142 ABb pair with future observations. HD 284149 ABb therefore adds to the short list of brown dwarf companions in circumbinary configuration (Bonavita et al. 2016), supporting their conclusion that brown dwarfs in wide circumbinary orbits occur with a similar frequency with respect to around single stars.

## Acknowledgements

We thank the anonymous referee for extensive feedback that significantly improved the clarity of the paper. This research made use of the Montreal Brown Dwarf and Exoplanet Spectral Library, maintained by Jonathan Gagné. This work has made use of data from the European Space Agency (ESA) mission *Gaia* (<http://www.cosmos.esa.int/gaia>), processed by the *Gaia* Data Processing and Analysis Consortium (DPAC, <http://www.cosmos.esa.int/web/gaia/dpac/consortium>). Funding for the DPAC has been provided by national institutions, in particular the institutions participating in the *Gaia* Multilateral Agreement. SPHERE is an instrument designed and built by a consortium consisting of IPAG (Grenoble, France), MPIA (Heidelberg, Germany), LAM (Marseille, France), LESIA (Paris, France), Laboratoire Lagrange (Nice, France), INAF - Osservatorio di Padova (Italy), Observatoire Astronomique de l’Université de Genève (Switzerland), ETH Zurich (Switzerland), NOVA (Netherlands), ONERA (France) and ASTRON (Netherlands) in collaboration with ESO. SPHERE was funded by ESO, with additional contributions from CNRS (France), MPIA (Germany), INAF (Italy), FINES (Switzerland) and NOVA (Netherlands). SPHERE also received funding from the European Commission Sixth and Seventh Framework Programmes as part of the Optical In-

<sup>8</sup> Given the nature of the two companions, the IAU nomenclature would require naming that system HD 284149 (AB)C, where C refers to the brown dwarf. As the BD companion was already known as HD 284149 b, we nonetheless decided to keep the previous nomenclature to avoid future confusion.

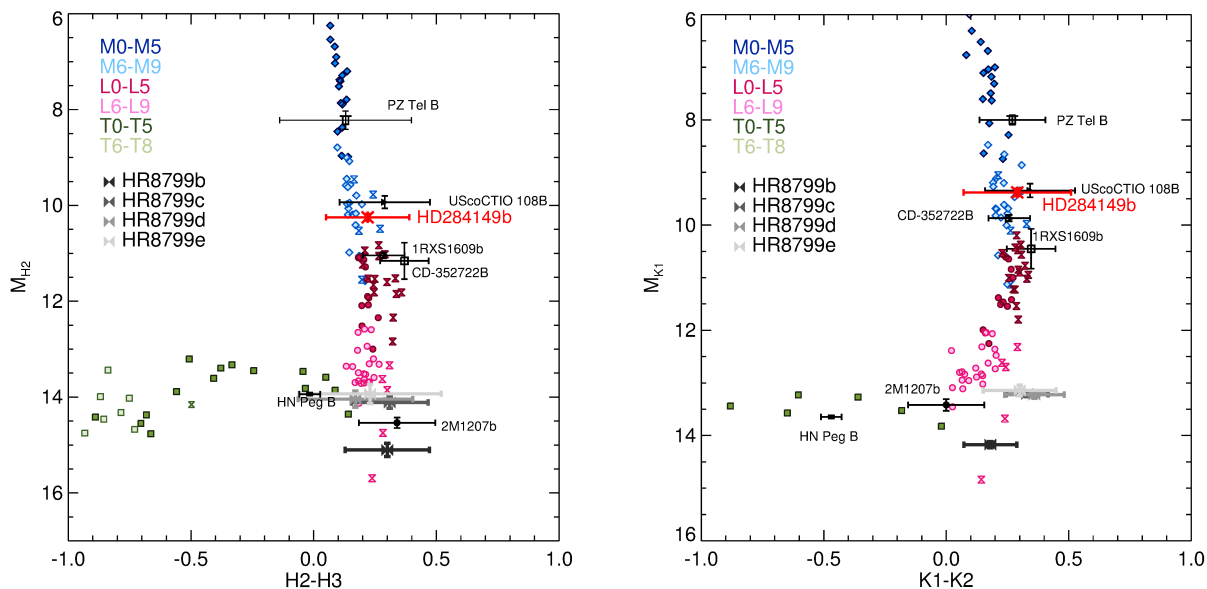


Fig. 13: Color–magnitude diagrams showing the position of HD 284149 b (red bow tie) relative to that of M, L and T field dwarfs and of young known companions, based on the H2-H3 photometry from the coronagraphic data (left panel) and the K1-K2 photometry from the non-coronagraphic data (right panel). See Section 4.1.1 for all the appropriate references and details on the construction of the plots.

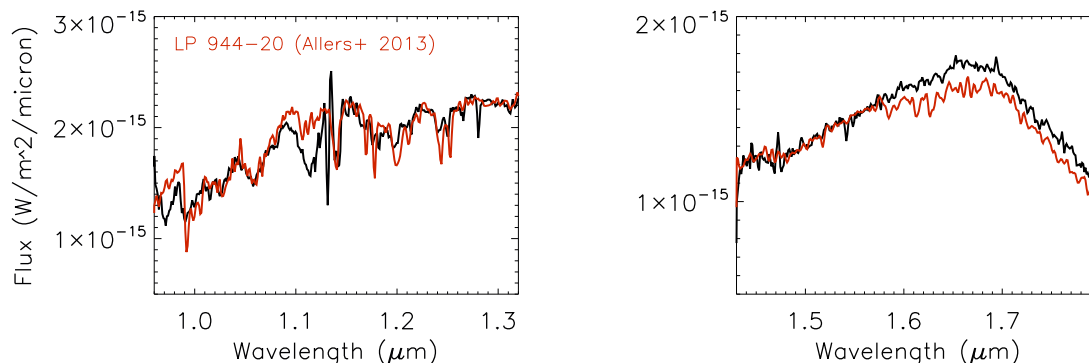


Fig. 14: Comparison of HD 284149 b with LP 944–20 from Allers & Liu (2013)

frared Coordination Network for Astronomy (OPTICON) under grant number RII3-Ct-2004-001566 for FP6 (2004-2008), grant number 226604 for FP7 (2009-2012) and grant number 312430 for FP7 (2013-2016). We acknowledge financial support from the Programme National de Planétologie (PNP) and the Programme National de Physique Stellaire (PNPS) of CNRS-INSU. Part of this work has been carried out within the frame of the National Centre for Competence in Research PlanetS supported by the Swiss National Science Foundation. S.D. acknowledges the financial support of the SNSF. This work has also been supported by a grant from the French Labex OSUG@2020 (Investissements d’avenir, ANR10 LABX56). We thank the anonymous referee for extensive feedback that significantly improved the clarity of the paper. We acknowledge support from the "Progetti Premiali" funding scheme of the Italian Ministry of Education, University, and Research. This work has made use of the SPHERE Data Centre, jointly operated by OSUG/IPAG (Grenoble), PYTHEAS/LAM/CeSAM (Mar-

seille), OCA/Lagrange (Nice) and Observatoire de Paris/LESIA (Paris).

## References

- Allard, F., Homeier, D., Freytag, B., & Sharp, C. M. 2012, in EAS Publications Series, Vol. 57, EAS Publications Series, ed. C. Reylé, C. Charbonnel, & M. Schultheis, 3–43
- Allers, K. N., Jaffe, D. T., Luhman, K. L., et al. 2007, *ApJ*, 657, 511
- Allers, K. N. & Liu, M. C. 2013, *ApJ*, 772, 79
- Allers, K. N., Liu, M. C., Shkolnik, E., et al. 2009, *ApJ*, 697, 824
- Amara, A. & Quanz, S. P. 2012, *Monthly Notices of the Royal Astronomical Society*, 427, 948
- Antichi, J., Dohlen, K., Gratton, R. G., et al. 2009, *ApJ*, 695, 1042
- Artigau, É., Gagné, J., Faherty, J., et al. 2015, *ApJ*, 806, 254
- Bailer-Jones, C. A. L. 2011, *MNRAS*, 411, 435
- Bailey, V., Meshkat, T., Reiter, M., et al. 2014a, *ApJ*, 780, L4
- Bailey, V., Meshkat, T., Reiter, M., et al. 2014b, *ApJL*, 780, L4
- Baraffe, I., Chabrier, G., Barman, T. S., Allard, F., & Hauschildt, P. H. 2003, *A&A*, 402, 701
- Bate, M. R., Bonnell, I. A., & Bromm, V. 2003, *MNRAS*, 339, 577
- Béjar, V. J. S., Zapatero Osorio, M. R., Pérez-Garrido, A., et al. 2008, *ApJ*, 673, L185

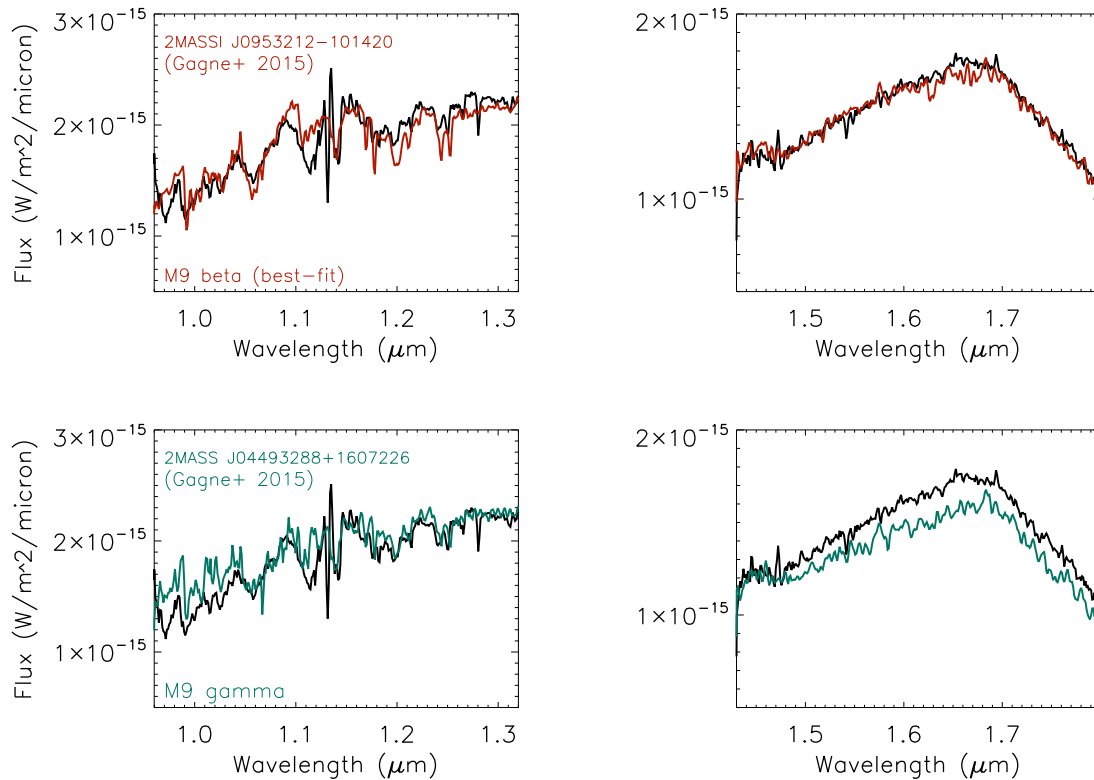


Fig. 15: Comparison of HD 284149 b with two M9-type brown dwarfs from the Montreal Spectral Library. While the global best fit is provided by the M9 $\beta$ , it is evident that individual spectral lines are too strong with respect to HD 284149 b, suggesting a lower gravity for this object (see the comparison with the M9 $\gamma$  spectrum).

- Bell, C. P. M., Mamajek, E. E., & Naylor, T. 2015, *MNRAS*, 454, 593
- Beuzit, J.-L., Feldt, M., Dohlen, K., et al. 2008, in *SPIE*, Vol. 7014, Ground-based and Airborne Instrumentation for Astronomy II, 701418
- Biller, B. A., Liu, M. C., Wahhaj, Z., et al. 2010, *ApJ*, 720, L82
- Bonavita, M., Daemgen, S., Desidera, S., et al. 2014, *ApJ*, 791, L40
- Bonavita, M., Desidera, S., Thalmann, C., et al. 2016, *A&A*, 593, A38
- Bonnefoy, M., Chauvin, G., Lagrange, A.-M., et al. 2014, *A&A*, 562, A127
- Bonnefoy, M., Zurlo, A., Baudino, J. L., et al. 2016, *A&A*, 587, A58
- Bowler, B. P., Liu, M. C., Mawet, D., et al. 2017, *AJ*, 153, 18
- Bressan, A., Marigo, P., Girardi, L., et al. 2012, *MNRAS*, 427, 127
- Brott, I. & Hauschildt, P. H. 2005, in *ESA Special Publication*, Vol. 576, The Three-Dimensional Universe with Gaia, ed. C. Turon, K. S. O'Flaherty, & M. A. C. Perryman, 565
- Burgasser, A. J. 2014, in *Astronomical Society of India Conference Series*, Vol. 11, *Astronomical Society of India Conference Series*
- Butters, O. W., West, R. G., Anderson, D. R., et al. 2010, *A&A*, 520, L10
- Carson, J., Thalmann, C., Janson, M., et al. 2013, *ApJ*, 763, L32
- Chauvin, G., Lagrange, A.-M., Dumas, C., et al. 2005a, *A&A*, 438, L25
- Chauvin, G., Lagrange, A.-M., Zuckerman, B., et al. 2005b, *A&A*, 438, L29
- Choi, J., Dotter, A., Conroy, C., et al. 2016, *ApJ*, 823, 102
- Claudi, R. U., Turatto, M., Gratton, R. G., et al. 2008, in *SPIE*, Vol. 7014, Ground-based and Airborne Instrumentation for Astronomy II, 70143E
- Daemgen, S., Bonavita, M., Jayawardhana, R., Lafrenière, D., & Janson, M. 2015, *ApJ*, 799, 155
- De Rosa, R. J., Patience, J., Ward-Duong, K., et al. 2014, *MNRAS*, 445, 3694
- Delorme, P., Gagné, J., Girard, J. H., et al. 2013, *A&A*, 553, L5
- Desidera, S., Covino, E., Messina, S., et al. 2015, *A&A*, 573, A126
- Dobson, A. K., Donahue, R. A., Radick, R. R., & Kadlec, K. L. 1990, in *Astronomical Society of the Pacific Conference Series*, Vol. 9, *Cool Stars, Stellar Systems, and the Sun*, ed. G. Wallerstein, 132–135
- Dohlen, K., Langlois, M., Saisse, M., et al. 2008, in *SPIE*, Vol. 7014, Ground-based and Airborne Instrumentation for Astronomy II, 70143L
- Donahue, R. A. & Baliunas, S. L. 1992, *ApJL*, 393, L63
- Dupuy, T. J., Forbrich, J., Rizzuto, A., et al. 2016, *ApJ*, 827, 23
- Dupuy, T. J. & Kraus, A. L. 2013, *Science*, 341, 1492
- Faherty, J. K., Burgasser, A. J., Walter, F. M., et al. 2012, *ApJ*, 752, 56
- Filippazzo, J. C., Rice, E. L., Faherty, J., et al. 2015, *ApJ*, 810, 158
- Forgan, D., Parker, R. J., & Rice, K. 2015, *MNRAS*, 447, 836
- Forgan, D. & Rice, K. 2013, *MNRAS*, 432, 3168
- Gagné, J., Faherty, J. K., Cruz, K. L., et al. 2015, *ApJs*, 219, 33
- Gaia Collaboration, Brown, A. G. A., Vallenari, A., et al. 2016a, *ArXiv e-prints*
- Gaia Collaboration, Brown, A. G. A., Vallenari, A., et al. 2016b, *A&A*, 595, A2
- Gauza, B., Béjar, V. J. S., Pérez-Garrido, A., et al. 2015a, *ApJ*, 804, 96
- Gauza, B., Béjar, V. J. S., Pérez-Garrido, A., et al. 2015b, *ApJ*, 804, 96
- Gizis, J. E., Allers, K. N., Liu, M. C., et al. 2015, *ApJ*, 799, 203
- Grankin, K. N., Artemenko, S. A., & Melnikov, S. Y. 2007, *Information Bulletin on Variable Stars*, 5752
- Harrington, R. S. & Dahn, C. C. 1980, *AJ*, 85, 454
- Horne, J. H. & Baliunas, S. L. 1986, *ApJ*, 302, 757
- Janson, M., Bonavita, M., Klahr, H., & Lafrenière, D. 2012, *ApJ*, 745, 4
- Jenkins, J. S., Ramsey, L. W., Jones, H. R. A., et al. 2009, *ApJ*, 704, 975
- Kirkpatrick, J. D. 2005, *ARAA*, 43, 195
- Kirkpatrick, J. D., Cushing, M. C., Gelino, C. R., et al. 2011, *ApJS*, 197, 19
- Kirkpatrick, J. D., Reid, I. N., Liebert, J., et al. 2000, *AJ*, 120, 447
- Kraus, A. L., Herczeg, G. J., Rizzuto, A. C., et al. 2017, *ApJ*, 838, 150
- Kraus, A. L., Shkolnik, E. L., Allers, K. N., & Liu, M. C. 2014, *AJ*, 147, 146
- Lachapelle, F.-R., Lafrenière, D., Gagné, J., et al. 2015, *ApJ*, 802, 61
- Lafrenière, D., Jayawardhana, R., & van Kerkwijk, M. H. 2010, *ApJ*, 719, 497
- Lagrange, A.-M., Bonnefoy, M., Chauvin, G., et al. 2010, *Science*, 329, 57
- Langlois, M., Vigan, A., Moutou, C., et al. 2013, in *Proceedings of the Third AO4ELT Conference*, ed. S. Esposito & L. Fini, 63
- Leggett, S. K., Allard, F., Dahn, C., et al. 2000, *ApJ*, 535, 965
- Liu, M. C., Dupuy, T. J., & Allers, K. N. 2016, *ApJ*, 833, 96
- Liu, M. C., Magnier, E. A., Deacon, N. R., et al. 2013, *ApJL*, 777, L20
- Luhman, K. L., Mamajek, E. E., Shukla, S. J., & Loutrel, N. P. 2017, *AJ*, 153, 46
- Mace, G. N., Kirkpatrick, J. D., Cushing, M. C., et al. 2013, *ApJS*, 205, 6
- Macintosh, B., Graham, J. R., Barman, T., et al. 2015, *Science*, 350, 64
- Maire, A.-L., Bonnefoy, M., Ginski, C., et al. 2016a, *A&A*, 587, A56
- Maire, A.-L., Langlois, M., Dohlen, K., et al. 2016b, in *SPIE*, Vol. 9908, Society of Photo-Optical Instrumentation Engineers (SPIE) Conference Series, 990834
- Makarov, V. V. & Kaplan, G. H. 2005, *AJ*, 129, 2420
- Marois, C., Correia, C., Galicher, R., et al. 2014, in *SPIE*, Vol. 9148, Adaptive Optics Systems IV, 91480U

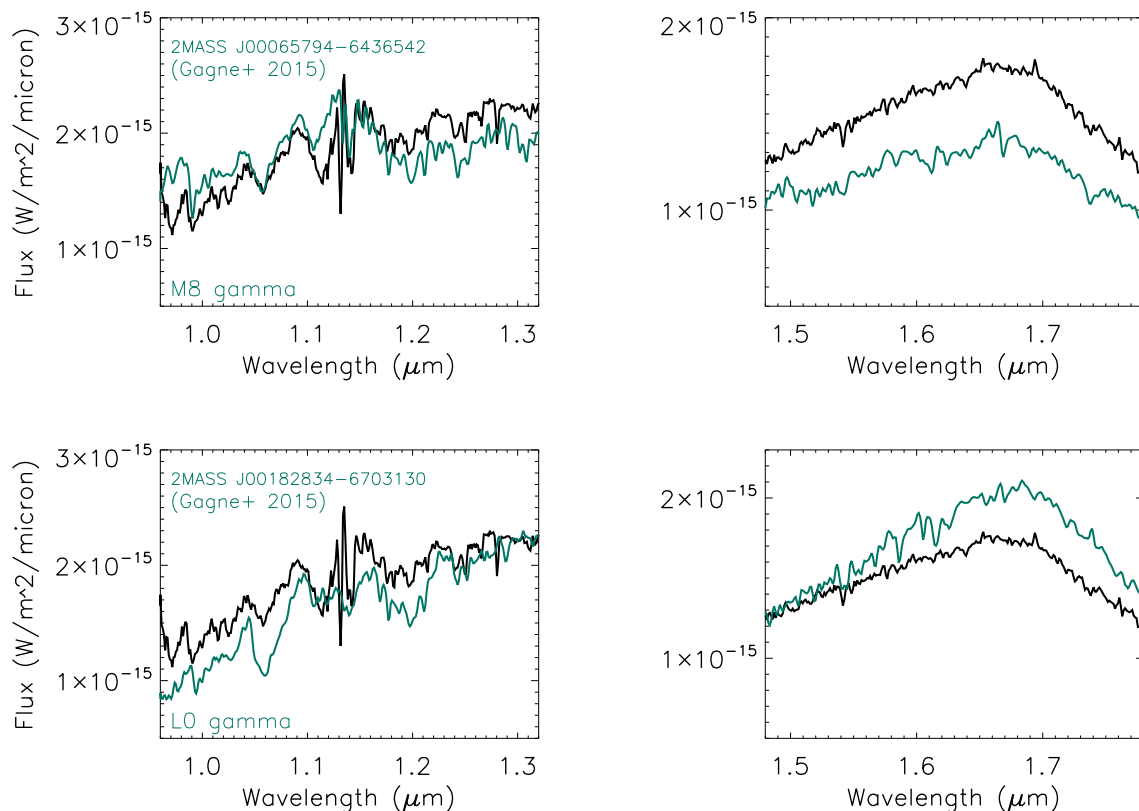


Fig. 16: Comparison of HD 284149 b with M8 and L0 young brown dwarfs from the Montreal Spectral Library (see text for discussion)

- Marois, C., Lafrenière, D., Doyon, R., Macintosh, B., & Nadeau, D. 2006a, *ApJ*, 641, 556
- Marois, C., Lafrenière, D., Macintosh, B., & Doyon, R. 2006b, *ApJ*, 647, 612
- Marois, C., Macintosh, B., Barman, T., et al. 2008, *Science*, 322, 1348
- Marois, C., Zuckerman, B., Konopacky, Q. M., Macintosh, B., & Barman, T. 2010, *Nature*, 468, 1080
- Martin, E. C., Mace, G. N., McLean, I. S., et al. 2017, *ApJ*, 838, 73
- McDonald, I., Zijlstra, A. A., & Boyer, M. L. 2012, *MNRAS*, 427, 343
- Meru, F. & Bate, M. R. 2010, *MNRAS*, 406, 2279
- Mesa, D., Gratton, R., Zurlo, A., et al. 2015, *A&A*, 576, A121
- Mesa, D., Vigan, A., D'Orazi, V., et al. 2016a, *ArXiv e-prints*
- Mesa, D., Vigan, A., D'Orazi, V., et al. 2016b, *A&A*, 593, A119
- Messina, S. & Guinan, E. F. 2003, *A&A*, 409, 1017
- Messina, S., Lanzafame, A. C., Feiden, G. A., et al. 2016, *ArXiv e-prints*: 1607.06634
- Naud, M.-E., Artigau, É., Malo, L., et al. 2014, *ApJ*, 787, 5
- Nguyen, D. C., Brandeker, A., van Kerkwijk, M. H., & Jayawardhana, R. 2012, *ApJ*, 745, 119
- Patience, J., King, R. R., de Rosa, R. J., & Marois, C. 2010, *A&A*, 517, A76
- Pavlov, A., Möller-Nilsson, O., Feldt, M., et al. 2008, in *SPIE*, Vol. 7019, *Advanced Software and Control for Astronomy II*, 701939
- Pearce, T. D., Wyatt, M. C., & Kennedy, G. M. 2014, *MNRAS*, 437, 2686
- Pecaut, M. J. & Mamajek, E. E. 2013, *ApJs*, 208, 9
- Pecaut, M. J. & Mamajek, E. E. 2016, *MNRAS*, 461, 794
- Pojmanski, G. 1997, *ACA*, 47, 467
- Rajan, A., Rameau, J., De Rosa, R. J., et al. 2017, *AJ*, 154, 10
- Rameau, J., Chauvin, G., Lagrange, A.-M., et al. 2013, *ApJL*, 772, L15
- Samland, M., Mollière, P., Bonnefoy, M., et al. 2017, *A&A*, 603, A57
- Scargle, J. D. 1982, *ApJ*, 263, 835
- Schneider, A. C., Cushing, M. C., Kirkpatrick, J. D., et al. 2015, *ApJ*, 804, 92
- Sivaramakrishnan, A. & Oppenheimer, B. R. 2006, *ApJ*, 647, 620
- Skrutskie, M. F., Cutri, R. M., Stiening, R., et al. 2006, *AJ*, 131, 1163
- Sommer, R., Pueyo, L., & Larkin, J. 2012, *ApJL*, 755, L28
- Stone, J. M., Skemer, A. J., Kratter, K. M., et al. 2016a, *ApJL*, 818, L12
- Stone, J. M., Skemer, A. J., Kratter, K. M., et al. 2016b, *ApJL*, 818, L12
- Thalmann, C., Schmid, H. M., Boccaletti, A., et al. 2008, in *SPIE*, Vol. 7014, *Ground-based and Airborne Instrumentation for Astronomy II*, 70143F
- van Leeuwen, F. 2007, *A&A*, 474, 653
- Vigan, A. 2016, *SILSS: SPHERE/IRDIS Long-Slit Spectroscopy pipeline*, *Astrophysics Source Code Library*
- Vigan, A., Bonavita, M., Biller, B., et al. 2017, *ArXiv e-prints*
- Vigan, A., Bonnefoy, M., Ginski, C., et al. 2016, *A&A*, 587, A55
- Vigan, A., Langlois, M., Moutou, C., & Dohlen, K. 2008, *A&A*, 489, 1345
- Vigan, A., Moutou, C., Langlois, M., et al. 2010, *MNRAS*, 407, 71
- Wagner, K., Apai, D., Kasper, M., et al. 2016, *Science*, 353, 673
- Wahhaj, Z., Liu, M. C., Biller, B. A., et al. 2011a, *ApJ*, 729, 139
- Wahhaj, Z., Liu, M. C., Biller, B. A., et al. 2011b, *ApJ*, 729, 139
- Wichmann, R., Torres, G., Melo, C. H. F., et al. 2000, *A&A*, 359, 181
- Wright, E. L., Eisenhardt, P. R. M., Mainzer, A. K., et al. 2010, *AJ*, 140, 1868
- Zacharias, N., Monet, D. G., Levine, S. E., et al. 2004, in *Bulletin of the American Astronomical Society*, Vol. 36, *American Astronomical Society Meeting Abstracts*, 1418
- Zapatero Osorio, M. R., Béjar, V. J. S., Miles-Pérez, P. A., et al. 2014, *A&A*, 568, A6
- Zurlo, A., Vigan, A., Galicher, R., et al. 2016, *A&A*, 587, A57
- Zurlo, A., Vigan, A., Mesa, D., et al. 2014, *A&A*, 572, A85